

Assessment of OTT Parsivel² Raindrop Fall Speed Measurements

RUPAYAN SAHA^a AND FIRAT Y. TESTIK^{a,b}

^a School of Civil and Environmental Engineering, and Construction Management, The University of Texas at San Antonio, San Antonio, Texas

^b Department of Mechanical Engineering, The University of Texas at San Antonio, San Antonio, Texas

(Manuscript received 11 August 2022, in final form 25 January 2023, accepted 31 January 2023)

ABSTRACT: This study was to assess the raindrop fall speed measurement capabilities of OTT Parsivel² disdrometer through comparisons with measurements of a collocated High-speed Optical Disdrometer (HOD). Raindrop fall speed is often assumed to be terminal in relevant hydrological and meteorological applications, and generally predicted using terminal speed–raindrop size relationships obtained from laboratory observations. Nevertheless, recent field studies have revealed that other factors (e.g., wind, turbulence, raindrop oscillations, and collisions) significantly influence raindrop fall speed, necessitating accurate fall speed measurements for many applications instead of reliance on laboratory-based terminal speed predictions. Field observations in this study covered rainfall events with a variety of environmental conditions, including light, moderate, and heavy rainfall events. This study also involved rigorous laboratory experiments to faithfully identify the internal filtering and calculation algorithm of OTT Parsivel². Our assessments revealed that, for the smaller diameter bins, Parsivel² filters out many of the observed raindrops that fall faster than predicted terminal speeds, bringing down the mean fall speed for those size bins without observational evidence. Furthermore, Parsivel² fall speed measurements exhibited notable artificial bell-shaped deviations from the predicted terminal speeds toward subterminal fall starting at around 1 mm diameter raindrops with peak deviations around 1.625 mm diameter bin. Such bell-shaped fall speed deviation patterns were not present in collocated HOD measurements. Assessment results along with the faithfully identified Parsivel² algorithm are presented with discussions on implications on reported raindrop size distributions (DSD) and rainfall kinetic energy.

KEYWORDS: Rainfall; In situ atmospheric observations; Instrumentation/sensors

1. Introduction

Accurate and precise raindrop fall speed measurements have significant importance for many applications including those related to radar meteorology, agriculture, atmospheric physics, and hydrology. For example, Dual-Frequency Precipitation Radar (DPR) uses raindrop fall speed measurements to characterize the type of rain for assisting flood forecasting and warning system (Awaka et al. 2016). Raindrop fall speed is an important microphysical quantity also for calculating other rainfall quantities such as raindrop size distribution (DSD) and kinetic energy. In various rainfall applications, it is commonly assumed that raindrops fall at predicted terminal speeds based on laboratory-observed terminal speed–size relationships (e.g., Cotton and Anthes 1992; Testik and Barros 2007; Pruppacher and Klett 2012). However, observations have shown that, in addition to raindrop size, there are other factors such as wind, turbulence, raindrop collisions, and oscillations (Montero-Martínez et al. 2009; Montero-Martínez and García-García 2016; Pinsky and Khain 1996; Testik et al. 2006) that significantly affect raindrop fall speeds. Therefore, precise and accurate raindrop fall speed measurements are essential.

Disdrometers are instruments that are used to measure raindrop size, fall speed, DSD, and often rain rate. There is a wide range of applications for disdrometer measurements.

For example, disdrometer measurements have been used for quality control in quantitative precipitation estimations using dual-polarization radars (e.g., Aoki et al. 2016). There are different types of disdrometers with different working principles for raindrop measurements. Both Parsivel² and High-speed Optical Disdrometer (HOD) are optical-type disdrometers with differing optical sensor technologies to measure the raindrop characteristics. HOD is an image-based optical disdrometer that uses a high-speed camera and light-emitting diode (LED) light to capture the silhouettes of raindrops to measure raindrop characteristics using image processing techniques. On the other hand, Parsivel² is a laser-based optical disdrometer that measures raindrop size and speed using voltage changes as the raindrops traverse through the laser sheet. Differing working principles and sensor technologies lead to differing measurement limitations and accuracy issues for certain raindrop size and fall speed ranges. Furthermore, these disdrometers may face different calibration issues (e.g., Lanza et al. 2021; Baire et al. 2022). In this study, we assessed raindrop fall speed measurements by Parsivel² disdrometer, which is manufactured by OTT Hydromet Inc. as their second generation of particle size velocity disdrometer (Parsivel²). This instrument was selected for this study because of its widespread use among researchers due to its simple operation, robust, and low-cost features, and also because of availability of a large volume of data from this instrument. A simple online search of publications with optical disdrometers between 2000 and 2022 revealed that Parsivel was mentioned in more than half of the first 200 research documents. Despite its

Corresponding author: Firat Y. Testik, firat.testik@utsa.edu

DOI: 10.1175/JTECH-D-22-0091.1

© 2023 American Meteorological Society. For information regarding reuse of this content and general copyright information, consult the [AMS Copyright Policy](http://www.ametsoc.org/PUBSReuseLicenses) (www.ametsoc.org/PUBSReuseLicenses).

popularity, there is a limited number of investigations on its measurement capabilities, especially in terms of accuracy of fall speed measurements (Angulo-Martínez and Barros 2015; Lin et al. 2021; Park et al. 2017; Tokay et al. 2014).

OTT Parsivel disdrometers have first (Parsivel¹) and second (Parsivel² used in this study) generations. Parsivel was first developed by PM Tech AG, Pfinztal, Germany, which was later transferred to OTT Hydromet, Kempten, Germany, in 2004. OTT Hydromet modified the instrument as Parsivel¹ in 2005. The OTT and PM Tech models were distinct in key ways. The PM Tech and OTT Parsivel¹ output voltages were sampled at 10 and 50 kHz, respectively (Battaglia et al. 2010). In comparison to the PM Tech Parsivel, the OTT Parsivel¹ used a laser sensor that has reduced homogeneity across the laser beam (Tokay et al. 2013). The World Meteorological Organization conducted a 1.5-yr field experimental campaign in central Italy with 30 rain gauges and optical disdrometers including Parsivel¹ (Lanza and Vuerich 2009). In comparison to selected reference gauges in this campaign, Parsivel¹ received a 3 out of 5 rating for 1-min rain-rate measurements. Lanza and Vuerich (2009) reported that Parsivel¹ overestimated rain intensity, and the overestimation worsened with increasing rain rate. In 2011, OTT launched Parsivel², a new model of the Parsivel¹. Parsivel² is a new design, in which the electronics are housed in the sleeve rather than the two heads of the sensor as was the case for Parsivel¹. According to the manufacturer, the main improvement is the use of a more advanced laser sensor and better homogeneity in the laser sheet for raindrop measurements. Manufacturer reported measurement accuracies for raindrops up to 2 mm in diameter are ± 1 size class for Parsivel² and ± 3 size classes for Parsivel¹, and for raindrops that are larger than 2 mm in diameter, the reported measurement accuracies are ± 0.5 size class for Parsivel² and ± 2 size classes for Parsivel¹.

Previous studies have demonstrated that both Parsivel¹ and Parsivel² are susceptible to errors in raindrop concentration measurements, particularly for small ($D < 1$ mm) and large ($D > 4$ mm) raindrop size bins (Thurai et al. 2011; Tokay et al. 2013; Raupach and Berne 2015; Park et al. 2017). Thurai et al. (2011) reported Parsivel¹'s overestimation of the number of large raindrops in terms of mass weighted mean diameter (D_m) by 20%–30% for higher rain rates (>20 mm h^{-1}) by comparing collocated measurements from a two-dimensional video disdrometer (2DVD) and a Parsivel¹. Moreover, by comparing Parsivel¹ measurements with collocated Joss-Waldvogel (JWD) and 2DVD disdrometer measurements, Tokay et al. (2013) concluded that Parsivel¹ underestimated the number of small raindrops ($D < 0.76$ mm) and measured relatively higher raindrop concentration when diameter is larger than 2.44 mm for rain rates and raindrop counts more than 2.5 mm h^{-1} and 400 drops min^{-1} , respectively. More recently, Raupach and Berne (2015) and Park et al. (2017) evaluated the second-generation Parsivel² measurements using a collocated 2DVD disdrometer and found that, during high intensity rain (>20 mm h^{-1}), Parsivel² still has significant biases that cause it to overestimate the quantity of large raindrops while underestimating the number of small raindrops.

In addition to the aforementioned sampling uncertainty, there are other previously reported Parsivel measurement issues related to, for example, the laser beam, raindrop splash, wind, coexistence of multiple raindrops in the laser beam, and raindrop fall through the edge of the laser sheet known as margin fallers (Habib et al. 2001; Kruger and Krajewski 2002; Loh et al. 2019; Nešpor et al. 2000; Raupach and Berne 2015; Tokay et al. 2001; Yu et al. 2016). When compared to the predicted terminal speeds, Upton and Brawn (2008) reported underestimations in Parsivel¹ fall speed measurements, especially for midsize raindrops ($D = 1$ –3 mm). While the study by Upton and Brawn was for the earlier version of Parsivel (Parsivel¹), Tokay et al. (2014) and Angulo-Martínez et al. (2018) showed that this measured fall speed behavior is systematic for raindrops 1.09 mm and larger also for the current Parsivel version (Parsivel²). Tokay et al. (2014) reported that the difference between the mean Parsivel² measured and predicted terminal fall speeds for 1.09 mm raindrops was approximately 1 m s^{-1} and the difference decreased with increasing raindrop size. Consequently, they suggested the use of terminal speed predictions in calculating DSD and rainfall parameters to alleviate the error. Another potential source for measurement issues is related to the assignment of Parsivel observations within preset size intervals (i.e., diameter/size bins) to the mean sizes of the corresponding intervals, compromising the measurement accuracies near the interval boundaries. Parsivel¹ was reported to be prone to this issue, known as the quantization error, particularly for size bins ≥ 2 mm (Yuter et al. 2006). It is important to emphasize that fall speed measurement inaccuracy has important effects. For example, systematic underestimation of fall speed may lead to increased equivalent volume drop concentration and radar reflectivity and decreased kinetic energy (Jaffrain and Berne 2011).

Friedrich et al. (2013) noted that particles falling oblique to the Parsivel measurement area (laser sheet) can be a cause for misclassification of fall speed. Their laboratory experiments showed increased concentration of larger drops (>3 mm) and decreased fall speeds when drops fall oblique to the measurement area. Friedrich et al. (2013) confirmed these laboratory findings in high wind speed and/or heavy rainfall events during Hurricane Ike in 2008 and convective storms, showing the influence of strong winds on particle size distributions measured by Parsivel¹ disdrometers. Raindrop shape deformation and oscillations may be another source of fall speed measurement uncertainty, especially for the case of large raindrops (Yu et al. 2016; Testik and Rahman 2016; Pei et al. 2014; Testik et al. 2006). Assumed oblate shapes of hydrometeors, hence inaccurate equivolume diameters, may also be a source of measurement uncertainty for Parsivel disdrometers (Battaglia et al. 2010).

Parsivel and other disdrometers use methodologies to filter out and correct erroneous measurements based on predicted terminal speeds (Jaffrain and Berne 2011; Tokay et al. 2013; Raupach and Berne 2015; Testik and Pei 2017). For example, Tokay et al. (2013) and Jaffrain and Berne (2011) removed raindrops exceeding $\pm 50\%$ and $\pm 60\%$ of the terminal speed predictions, respectively. There are a number of available relationships for terminal speed predictions in the literature.

Nevertheless, these predictions are mostly from laboratory observations of water drops in stagnant air (Beard 1977; Blanchard 1950; Epema and Riezebos 1983; Jayawardena and Rezaur 2000; Laws 1941; Gunn and Kinzer 1949, hereafter referred as GK49) and may not accurately represent the actual raindrop fall speeds during rainfall events under certain conditions (e.g., Hosking and Stow 1991; Montero-Martínez et al. 2009; Montero-Martínez and García-García 2016; Testik et al. 2006; Thurai et al. 2013). Therefore, filtering, while essential due to instrumental limitations, has the potential to result in underestimation of the number of raindrops and masking of the signatures of different microphysical processes. Therefore, identification and improvement of instrumental limitations has significant importance.

In this paper, we assess raindrop fall speed measurement capabilities of OTT Parsivel² by comparing values with HOD measurements. Brief descriptions of Parsivel² and HOD disdrometers are provided in section 2, followed by an overview of our experimental sites, observed rainfall events, methodologies, and identification of Parsivel² algorithm for raindrop fall speed measurements. Results, including statistical comparisons among Parsivel² and HOD measurements and predicted terminal speeds by an empirical fit equation based on GK49 laboratory data, as well as discussions on the effects of Parsivel² raindrop fall speed measurements on DSD observations and rainfall kinetic energy estimations are presented in section 3. Finally, conclusions of this study are provided in section 4.

2. Experimentation: Disdrometers, field site, and methodology

a. OTT Parsivel² and HOD disdrometers

Only a brief description of OTT Parsivel² is provided here and detailed descriptions of Parsivel² can be found in the literature (e.g., Angulo-Martínez et al. 2018; Park et al. 2017; Tokay et al. 2014). Parsivel² uses a 780 nm laser beam that forms a nominal measurement cross-sectional area of 54 cm^2 ($L = 180 \text{ mm}$ long, $W = 30 \text{ mm}$ wide, and $T = 1 \text{ mm}$ thick) to detect particles (OTT 2017). However, since particles partially passing through this nominal measurement area at the edges are not counted, the effective measurement area changes for each raindrop diameter bin as $L \times (W - D/2)$, where D represents raindrop diameter bins. When particles pass through the measurement area formed by the laser beam, a portion of the transmitted laser is blocked, resulting in a change in voltage in comparison to when the laser beam is free of particles. The amplitude of the voltage drop is used to determine the size of the particle whereas the duration of the voltage drop is used to determine the fall speed of the particle. In calculating fall speeds, Parsivel² also uses assumed particle axis ratios. According to Battaglia et al. (2010), Parsivel² assumes particles as spherical up to 1 mm, and as horizontally oriented oblate spheroids with axis ratios linearly varying from 1 to 0.7 between 1 and 5 mm and with a fixed axis ratio value of 0.7 for particles larger than 5 mm. These assumed axis ratio values

impose a notable potential to affect the accuracy of Parsivel² measurements during events with strong winds. Note that, given the outlined working principle, size of the measurement area greatly influences the probability of bias-inducing effects such as edge events (margin fallers) and overlapping hydrometeors (Angulo-Martínez et al. 2018). A larger measurement area, for instance, implies a higher chance of overlapping hydrometeors (i.e., multiple hydrometeors coexisting in the laser sheet at the same time and recorded as a single hydrometeor). This may cause missed hydrometeor observations, translating to a reduced hydrometeor count, precipitation amount and rate, and also recordings of larger than actual hydrometeor sizes with fall speeds that are unusually low. Parsivel² measures both solid and liquid precipitation. However, for the purposes of our study, here we consider Parsivel² for rainfall measurements.

According to the manufacturer's statement, Parsivel² measures raindrop characteristics for raindrops with diameters larger than 0.25 mm and during rainfall events with rain rates greater than 0.001 mm h^{-1} . Parsivel² validates the detected raindrops using its unknown internal algorithm and filters out those particles that are not validated as raindrops. Validated raindrops are assigned to a predefined 32×32 matrix, where rows and columns of the matrix indicate raindrop diameter and fall speed classes/bins, respectively. The diameter and fall speed bins have unequal intervals ranging from 0 to 26 mm and 0 to 22.4 m s^{-1} , respectively. Bin widths increase from 0.125 to 3 mm for diameter bins and 0.1 to 3.2 m s^{-1} for fall speed bins as raindrop diameter and fall speed bins increase. Parsivel² software does not provide individually measured raindrop diameter and fall speed values, but rather provides the number of raindrops in each of the predefined Parsivel² diameter and fall speed bins along with the average volume equivalent diameter and average particle speed of each bin. For this study, Parsivel² was connected to a CR1000 datalogger for automated data storage purposes. A computer program was developed using PC200W software to communicate between CR1000 and Parsivel². This program provided us the opportunity to extract all of the detected raindrop diameter and fall speed values captured by Parsivel² before they are processed by the Parsivel² internal algorithm for raindrop validation. This capability enabled us to conduct the analyses presented in this study.

Detailed information on the HOD can be found in Testik and Rahman (2016) and only a brief overview of this instrument is provided here. HOD is a recently developed research instrument with one of the design purposes being accurate hydrometeor fall speed observations. It is an optical-type disdrometer that consists of a high-speed camera, an LED light, and a sensor to trigger the camera once a hydrometeor (i.e., raindrop for this study) is detected in the measurement volume that is defined by the camera view frame and sensor detection area (see Testik and Rahman 2016). HOD captures successive high-speed (1000 frames per second for this study) images of each raindrop that passes through the measurement volume, providing both visual and quantitative information on raindrop dynamics. Using image processing techniques and the sequential raindrop images, HOD software determine

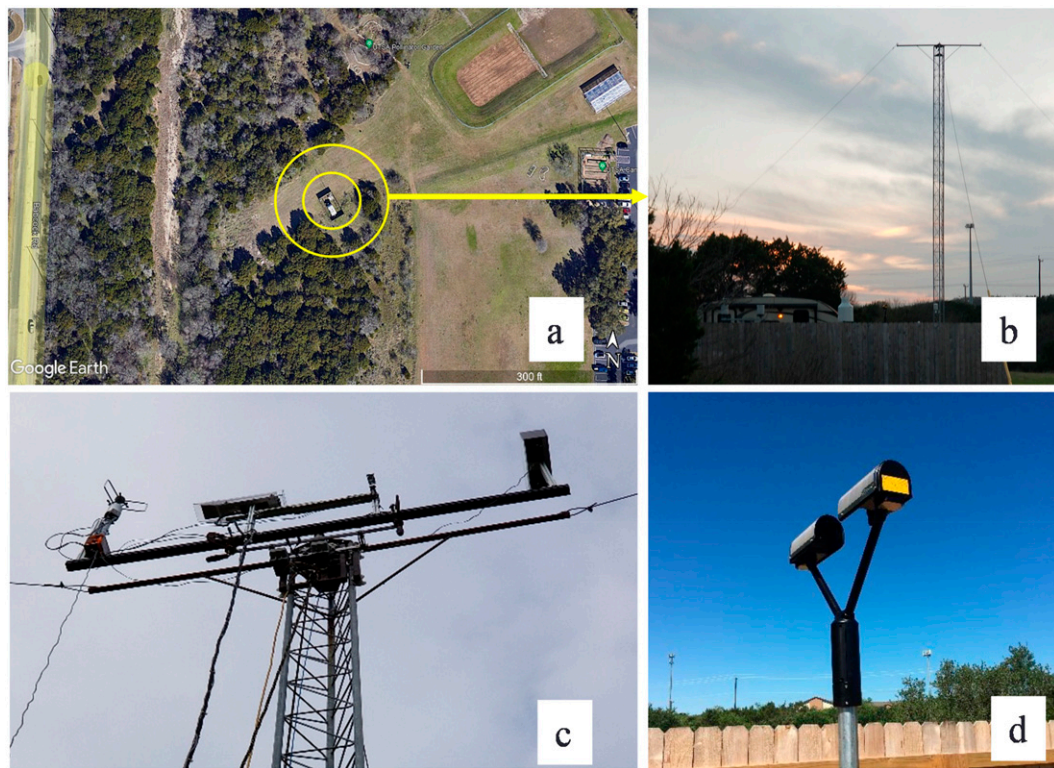


FIG. 1. (a) Satellite image of the field site (circled) and its surroundings. (b) Ground view of the field site and the meteorological tower. (c) Photograph of the HOD and 3D ultrasonic anemometer mounted at the top of the 10-m-tall tower. (d) Photograph of Parsivel² disdrometer mounted at 2 m above ground level.

the raindrop diameter and fall speed, which is calculated by utilizing the displacement of the centroid location of the same raindrop in two consecutive images, along with other microphysical quantities. These quantities for the same raindrop are measured multiple times depending on the number of sequential images, and are averaged for improved accuracy. For this study, HOD was set to record 10 images of each of the raindrops passing through the measurement volume. The measurement error of HOD for raindrops that are larger than 0.5 mm is less than approximately 10% of the raindrop diameter and reduces to approximately 2.9% as the raindrop diameter increases to 5 mm. Considering the measurement accuracy, HOD was set to detect only raindrops that are larger than 0.5 mm. Note that actual raindrop images captured by the HOD has an additional benefit of data quality controls, if needed, for raindrop size, speed, and shape. In this study, we used Parsivel² binning for HOD measurements of raindrop fall speed and size for adequate comparisons of the measurements from the two instruments.

b. Field site

Rainfall observations were conducted at our outdoor rainfall research laboratory (see Fig. 1) that is located in the west campus of The University of Texas at San Antonio, Texas, United States (coordinates and elevation: 29°34'43.19"N, 98°37'50.68"W, and 297 m above mean sea level, respectively). As can be seen in Fig. 1, the field site is situated within a flat

open suburban terrain that is free of tall trees and obstructions. The field site houses a 10-m-high meteorological tower that host the HOD and an R. M. Young 8500 3D ultrasonic anemometer. The site is also equipped with one OTT Parsivel² disdrometer, one OTT Pluvio² rain gauge, and two TB4 tipping-bucket rain gauges, all of them installed at 2 m above ground level.

c. Data collection and analysis methodology

Field experiments consisted of 6 different rainfall events for a total duration of 1456 min (Table 1). In this study, a rainfall event is defined as a period of continuous rain with an accumulation of at least 1 mm rain amount (Tokay et al. 2013). The successive rainfall events are separated from each other by a dry period of at least 1 h. These rainfall events cover a wide variety of light to heavy rainfall (0.01–102.96 mm h⁻¹) during calm to high wind conditions (0.08–7.59 m s⁻¹) and results from these events were consistent as discussed later in the article. Therefore, selected rainfall events were sufficient for conclusive findings. Ranges of rain intensity and wind speed values reported here and in Table 1 were determined using 1-min rain intensity and wind speed values. All of the aforementioned meteorological instruments were active during these events and collected a wealth of data.

We classify Parsivel² data in three levels as follows. Level 1 data consist of diameter and fall speed information for the

TABLE 1. Summary of the rainfall event characteristics observed for this study. ΔT = Rain duration. RI = Rain intensity measured by Parsivel². W = Wind speed measured by the 3D ultrasonic anemometer. T and RH represent temperature and relative humidity, respectively. Parsivel²-detected and -validated raindrop numbers are represented here by DR and VR, respectively.

Event No.	Date	ΔT (min)	RI_{avg} (mm h ⁻¹)	W_{avg} (m s ⁻¹)	RI range ^a (mm h ⁻¹)	W range ^a (m s ⁻¹)	T (°C)	RH (%)	DR	VR ^b (%)
1	16 Oct 2019	289	2.44	2.22	0.03–7.41	0.87–3.49	21	94	614 36	98
2	24 Oct 2019	319	11.88	5.55	0.02–102.96	1.66–7.59	13	88	178 517	90
3	20 Dec 2019	206	1.46	1.53	0.01–9.82	0.88–2.49	10	97	267 508	98
4	21 Mar 2020	290	1.83	1.87	0.01–8.17	0.08–3.13	11	95	332 253	99
5	15 May 2020	180	6.85	3.37	0.41–42.84	1.97–5.63	18	89	107 505	96
6	13 Oct 2021	172	12.73	2.53	0.05–74.96	0.69–5.48	22	97	107 496	97

^a RI and W ranges were calculated based on 1-min time resolution measurements during corresponding ΔT .

^b Percentages of validated raindrop numbers from detected raindrops.

raindrops detected by Parsivel² (i.e., raw data) as stored in the raindrop log file. Level 1 data have not been typically available to Parsivel² users as access to these data is not available through the instrument software provided by the manufacturer, but they were extracted in this study using a computer program written in PC200W software. The storage of level 1 data requires a large space because the program extracted signals from Parsivel² and stored up to a predefined number of cells in each minute whether Parsivel² detects any particles or not (e.g., rain or dry). Considering the heavy rain scenario and the limitation of the datalogger scan rate, we set the program to extract diameter and fall speed information for up to 2500 detected particles each minute. This setup generated large datasets from level 1 during long periods of rain. To resolve this storage issue, we installed a Compact Flash Memory Module (CFM100) with CR1000 datalogger. Level 2 data consist of raindrop counts for the validated raindrops in each bin of the 32 × 32 Parsivel² diameter–fall speed matrix. Level 2 data are derived by Parsivel² software using an internal unknown algorithm from level 1 data by filtering out some of the level 1 data and validating the rest of the raindrop data as level 2 data. Parsivel² users have access to level 2 data through the instrument's software. Level 3 data consist of average raindrop fall speeds for each diameter bin, DSD, integral rainfall parameters (rain rate and amount) that are calculated by Parsivel² software using level 2 data. Level 3 data are provided to the Parsivel² users as a readymade dataset. In addition, we introduced a new data level, which was not part of Parsivel² data collection and processing steps, and called this data level as “pseudo level 2” (described later in the text).

Using level 1 data from laboratory experiments, we were able to faithfully identify the Parsivel² internal algorithm to transform the data from level 1 to level 2. We refer to this portion of the internal algorithm as the “Parsivel² filtering matrix” (which is provided in Fig. 3 later). To identify the Parsivel² filtering matrix, we conducted laboratory experiments with a large number of water drops ($\approx 1\,000\,000$) generated using a pressurized hose (Fig. 2), covering a wide range of drop sizes (0.1–20 mm) and fall speeds (0.1–20 m s⁻¹). It is important to note here that we did not generate drops with controlled sizes and fall speeds. Our goal for the laboratory experiments was not to test the accuracy/uncertainty of Parsivel²

measurements for drop diameter and fall speed; hence, accuracy of the generated drop sizes and/or terminal and nonterminal fall were not of importance for this study. Instead, since our primary goal for the laboratory experiments was mainly to identify the detected (level 1) and validated (level 2) drops by Parsivel², we generated as many drops as possible that span a wide range of characteristics (i.e., size and speed) to reveal the Parsivel² drop validation criteria for the detected drops. Parsivel² readings from these experiments included both level 1 and level 2 data in each minute. Parsivel² level 1 data clearly showed that drops with different size and fall speed combinations were generated in our laboratory experiments, including those with small size and fast fall speeds that are eliminated by Parsivel² filtering matrix as discussed later in the article. Using level 1 data with detected drops, we constructed the 32 × 32 drop diameter and fall speed bin matrix for each minute of observations. Detailed comparisons of the 32 × 32 matrices for level 1 data for detected drops and for level 2 data for validated drops provided by Parsivel² software revealed Parsivel² filtering matrix for validation of raindrops when transforming data from level 1 to level 2. Figure 3 shows how the Parsivel² filtering matrix maps out diameter and fall speed bin combinations for validating the observed particles as raindrops. The results

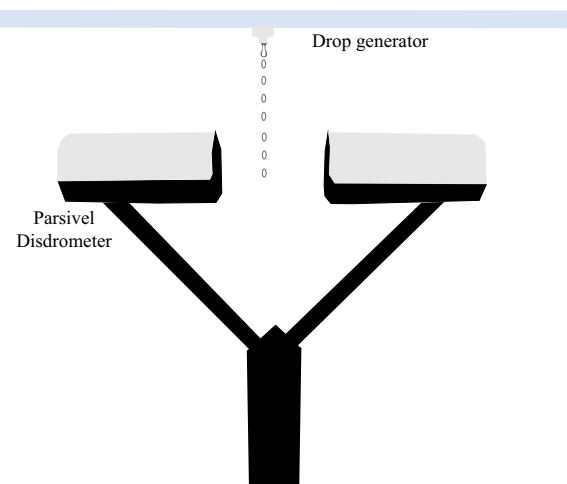


FIG. 2. Illustrative schematic of the laboratory experimental setup that was used to identify the Parsivel² filtering matrix.

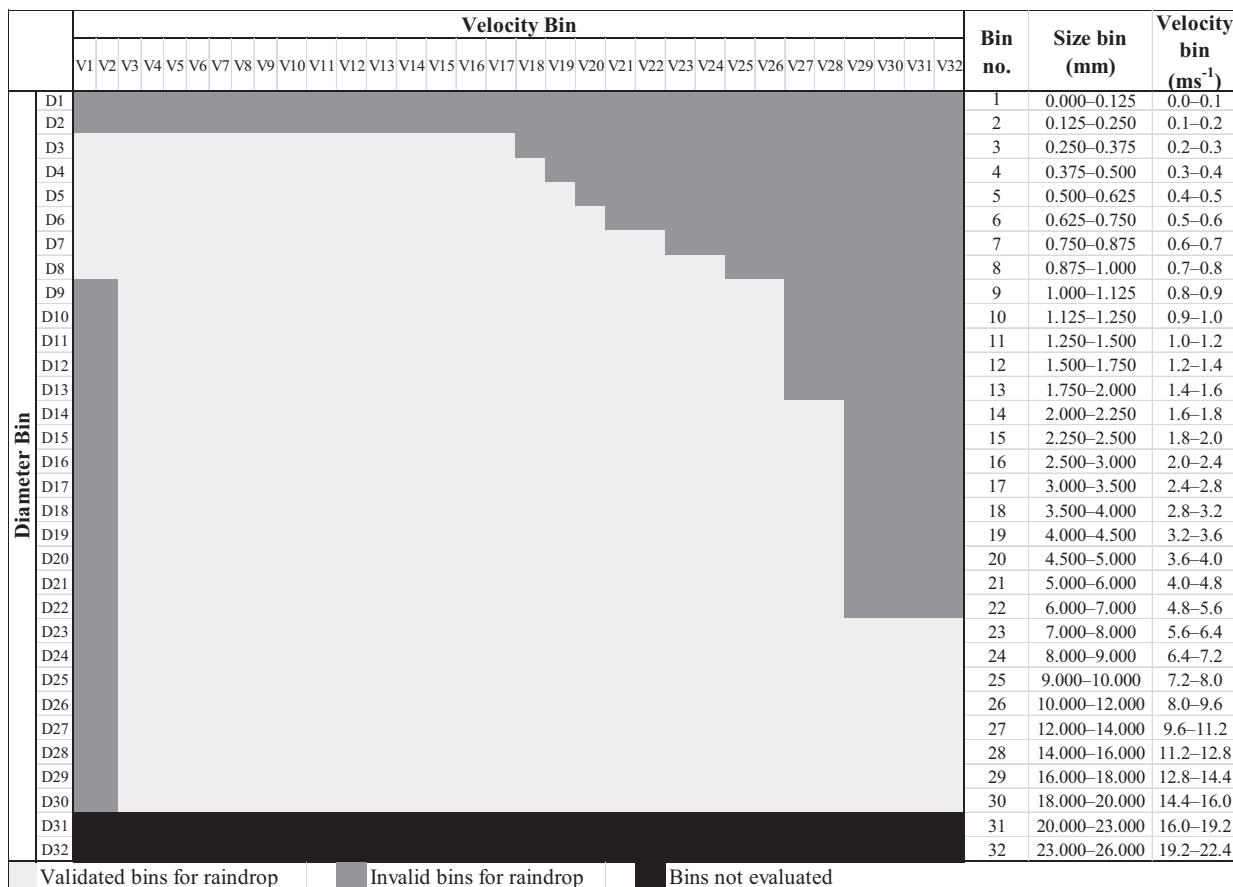


FIG. 3. Visualization of the Parsivel² filtering matrix to validate the detected particles as raindrops as part of the Parsivel² internal algorithm. Raindrops in light-gray-colored cells/bins are validated and those in dark-gray-colored bins are filtered out. Black-colored bins were not evaluated in this study. Parsivel² raindrop size and fall speed bins are also presented on the right side of the matrix.

from these laboratory experiments were also verified through rainfall observations at our field site.

Documentation of the Parsivel² filtering matrix enabled us to faithfully identify Parsivel²'s fall speed calculation algorithm. To identify Parsivel²'s fall speed calculation algorithm, we analyzed Parsivel² given average fall speed for each diameter bin (level 3) and fall speed of each validated raindrop that were distinguished from detected raindrops by the Parsivel² filtering matrix. Considering the number of validated raindrops and midvalue of respective fall speed bin, we calculated weighted-average fall speeds for each diameter bin (represented by open circles in Fig. 4) and compared with Parsivel² given average fall speeds of each diameter bin (level 3, represented by open squares in Fig. 4) in Fig. 4. As can be seen in this figure, open circles representing fall speeds that we calculated using the abovementioned procedure and open squares representing fall speeds reported by Parsivel² level 3 data overlapped precisely for each of the diameter bins. This comparison in Fig. 4 revealed that Parsivel² utilizes midvalue of respective fall speed bin, rather than individual raindrop fall speeds, for calculating average fall speed of each diameter bin in level 3. In this study,

in addition to the Parsivel² provided data levels, we included an additional data level, which we called "pseudo level 2." Pseudo level 2 data (represented by open triangles in Fig. 4) include the average fall speeds for each of the predefined diameter bins that are calculated by averaging the fall speed measurements from level 1 data for all of the raindrops in the corresponding diameter bins and validated through the Parsivel² filtering matrix. Level 2 and pseudo level 2 data differ such that while level 2 data provide only the number of raindrops in each of the predefined diameter and velocity bins and they are available through Parsivel² software, pseudo level 2 data provide the average fall speeds of the validated raindrops in each of the diameter bins using the individual raindrop fall speed measurements from level 1 data and are not available through Parsivel² software. Figure 4 also exhibits that pseudo level 2 fall speed values differ from level 3 fall speed values, and the differences become more pronounced for the larger raindrop fall speeds. The observed difference in fall speeds by pseudo level 2 and level 3 data was due to the nonuniform widths of predefined Parsivel² fall speed bins, which increase with increasing fall speed values (see Fig. 3). Using midvalues of predefined fall speed bins instead of average fall speeds of

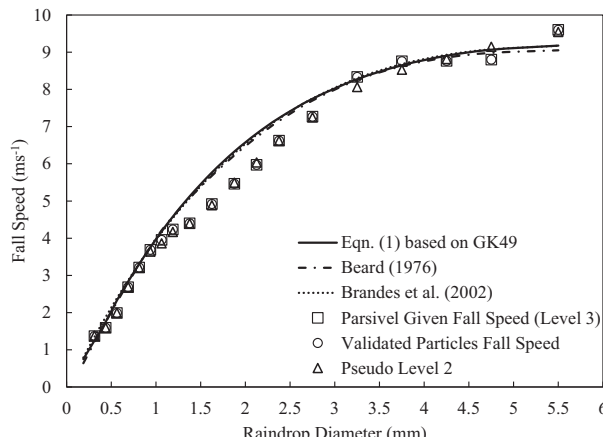


FIG. 4. Comparison of Parsivel² given average fall speed (level 3, open squares), pseudo level 2 (open triangles), and fall speeds that we calculated for the validated particles (open circles) to identify Parsivel² fall speed calculation algorithm. Raindrop terminal speed predictions by Eq. (1) based on GK49, Beard (1976), and Brandes et al. (2002) are represented by solid, dash-dotted, and dotted lines, respectively (see the legend).

raindrops within the given bin enhances the quantization error. This error would be particularly pronounced for the larger bin widths and bins with smaller number of raindrops as observed in Fig. 4. In this figure, we present terminal speed predictions using an empirical fit equation to GK49 laboratory data [see Eq. (1)] along with two other well-accepted terminal speed parameterizations, specifically by Beard (1976) and Brandes et al. (2002). This was to provide a visual comparison among terminal speed predictions by different parameterizations. The predictions by the empirical equation in Eq. (1) are within $\pm 1\%$ of the terminal speed measurements by GK49 for water drops within the diameter range of 0.5–6.0 mm:

$$V_t = 0.0623D^3 - 0.9481D^2 + 5.0403D - 0.2054. \quad (1)$$

Here, V_t is the terminal speed prediction (in m s^{-1}) and D is drop diameter (in mm). Furthermore, we conducted paired t test among predicted terminal speed predictions by the above-mentioned parameterizations with 0.05 significance level, which indicated that the mean differences among the predicted terminal speeds were not statistically significant (p value > 0.05). As such, for the rest of this article, we only considered predicted raindrop terminal speeds by Eq. (1) for comparisons with observed raindrop fall speeds, except in Table 2, where terminal speeds prediction by both Eq. (1) and Beard (1976) were considered for statistical comparisons with Parsivel² and HOD measurements.

To demonstrate the impact of Parsivel² filtering matrix that is implemented by Parsivel² by default, we compared the average raindrop fall speeds of Parsivel² detected (level 1) and validated (pseudo level 2) raindrops for each diameter bin (Fig. 5). Here, we used pseudo level 2 data because level 2 data did not provide the actual fall speed measurements, but

instead provided only the numbers of validated raindrops in each diameter and velocity bins as described earlier. Due to low signal-to-noise ratio, Parsivel² internal algorithm removes data from the two smallest diameter bins ($D < 0.25 \text{ mm}$), and then Parsivel² filtering matrix is applied to the detected raindrops to validate them. Figure 5 reveals that Parsivel² filtering matrix artificially filters out the detected raindrops at the smaller end of the diameter bins ($D < 1 \text{ mm}$) and reduces the average fall speed values without any observational evidence. In this figure, it can also be seen that application of the Parsivel² filtering matrix does not cause fall speed alterations for the detected and validated raindrops for $D > 1 \text{ mm}$. Parsivel² filtering matrix was further investigated by implementing it to the HOD fall speed measurements for event 5, and the results are presented in Fig. 6. In this figure, deviations of fall speed observations from terminal speed predictions are presented both in percentages (primary vertical axis) and absolute values (secondary vertical axis). The reasoning behind presenting deviations in terms of both relative (%) and absolute deviations in the same graph was to demonstrate that the importance of the issue was not artificially increased by our choice of relative deviations in terms of percentages for the relevant figures in the rest of this article. This figure demonstrates that implementation of Parsivel² filtering matrix increases deviations of the HOD fall speed measurements from terminal fall speed predictions by Eq. (1) for the smaller end of the diameter spectrum ($D < 0.8125 \text{ mm}$) and showed no effect for the rest of the diameter spectrum. Once Parsivel² fall speed calculations were faithfully determined, we investigated Parsivel² fall speed measurement capabilities in comparisons with HOD measurements and terminal fall speed predictions by GK49 as discussed in the next section.

3. Results and discussion

Figure 7 presents a typical comparison of raindrop fall speed measurements by HOD and Parsivel² (level 1—for detected raindrops) along with terminal speed predictions by Eq. (1) for (Fig. 7a) event 5 on 15 May 2020 and (Fig. 7ab) averages of raindrop fall speed observations during all of the events tabulated in Table 1. Results of the statistical comparisons of fall speed measurements for event 5 are presented in Table 2 later. Event 5 presented in Fig. 7a consisted of about 200 min of rainfall observations, during which 10-min-averaged wind speed values ranged between 2 and 5.5 m s^{-1} . Note that only raindrop diameter bins with more than 10 raindrops were considered for comparisons presented in this study. While Parsivel² software does not present the smallest two diameter bins ($D < 0.25 \text{ mm}$) of the level 2 data due to accuracy considerations as noted earlier, in this comparison, we included all Parsivel² diameter bins (including the smallest two diameter bins) as our comparison here is for level 1 data with all detected particles before implementation of the internal algorithm. This comparison revealed that, at the smaller end of the diameter bins, fall speeds of the raindrops detected by Parsivel² were much faster than the predicted terminal speeds. While omission of the two diameter bins smaller than 0.25 mm nulls the need for detailed considerations for those

TABLE 2. Results of one-sample and two-sample t tests for terminal speed predictions, and HOD and Parsivel² raindrop fall speed measurements for event 5. Mean, standard deviation, and number of observed raindrops for each diameter bin are also included. D represents the midsize of the diameter bin. $\mu_{v_f}^{\text{HOD}}$ and $\mu_{v_f}^{\text{Parsivel}}$ represent HOD- and Parsivel²-measured mean raindrop fall speeds, respectively. N_{HOD} and N_{Parsivel} represent HOD- and Parsivel²-measured number of raindrops, respectively. $\sigma_{v_f}^{\text{HOD}}$ and $\sigma_{v_f}^{\text{Parsivel}}$ represent standard deviation of HOD- and Parsivel²-measured raindrop fall speeds, respectively. Terminal speed predicted by Eq. (1) based on GK49 and by Beard (1976) are represented as V_{t_1} and V_{t_2} , respectively.

D (mm)	V_{t_1} (m s ⁻¹)	V_{t_2} (m s ⁻¹)	N_{v_f}	HOD			Parsivel ²		
				$\mu_{v_f}^{\text{HOD}}$ (m s ⁻¹)	$\sigma_{v_f}^{\text{HOD}}$ (m s ⁻¹)	p value ^a	$\mu_{v_f}^{\text{Parsivel}}$ (m s ⁻¹)	N_{Parsivel}	$\sigma_{v_f}^{\text{Parsivel}}$ (m s ⁻¹)
0.313	1.250	1.199	—	—	—	—	1.597	3655	0.583
0.438	1.750	1.744	—	—	—	—	1.814	8459	0.633
0.563	2.325	2.276	2,011	223	0.910	0.000	2.155	10290	0.631
0.688	2.828	2.794	2,794	180	1.080	0.673	0.996	2,601	10896
0.813	3.306	3.294	3,211	212	0.901	0.126	0.186	3,080	11836
0.938	3.756	3.766	3,667	235	0.770	0.078	0.050	3,453	12070
1.063	4.178	4.206	3,956	244	0.707	0.000	0.000	3,762	10578
1.188	4.574	4.574	4,523	264	0.706	0.242	0.240	3,994	7336
1.375	5.120	5.075	4,951	526	0.774	0.000	0.000	4,265	10922
1.625	5.765	5.678	5,468	434	0.757	0.000	0.000	4,696	7020
1.875	6.325	6.223	6,070	290	0.804	0.000	0.001	5,225	4201
2.125	6.810	6.714	6,555	203	0.850	0.000	0.008	5,771	2570
2.375	7.228	7.149	6,730	137	0.919	0.000	0.000	6,343	1612
2.750	7.747	7.700	7,417	129	0.977	0.000	0.001	6,943	1533
3.250	8.273	8.252	7,942	36	0.842	0.024	0.034	7,741	544
3.750	8.647	8.625	8,190	10	1.081	0.214	0.235	8,280	177
4.250	8.903	8.855	—	—	—	—	8,406	66	0.953

^a p value of one-sample t test with null hypothesis of $H_0: \mu_{v_f}^{\text{HOD}} = V_{t_1}$.

^b p value of one-sample t test with null hypothesis of $H_0: \mu_{v_f}^{\text{HOD}} = V_{t_2}$.

^c p value of one-sample t test with null hypothesis of $H_0: \mu_{v_f}^{\text{Parsivel}} = V_{t_1}$.

^d p value of one-sample t test with null hypothesis of $H_0: \mu_{v_f}^{\text{Parsivel}} = V_{t_2}$.

^e p value of two-sample t test with null hypothesis of $H_0: \mu_{v_f}^{\text{HOD}} = \mu_{v_f}^{\text{Parsivel}}$.

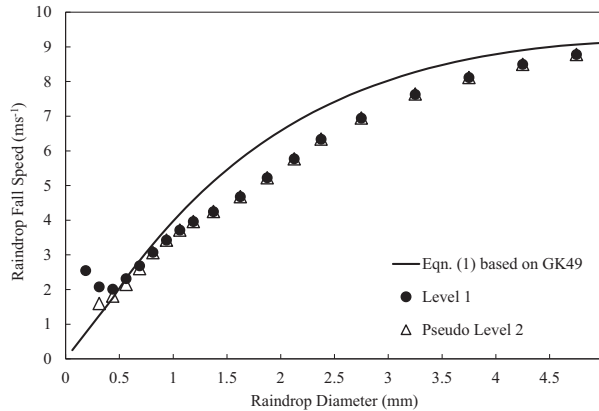


FIG. 5. Comparison of Parsivel² fall speed measurements for detected (level 1, solid circles) and validated raindrops (pseudo level 2, open triangles) with terminal fall speed predictions by Eq. (1) (solid line) to demonstrate the effects of Parsivel² internal algorithm.

two diameter bins, impact of Parsivel² filtering matrix implementation is evident for raindrop diameter bins between 0.25 and 0.5 mm, and care should be taken in microphysical interpretations using Parsivel² data for this size range. For raindrops between about 0.5 and 1 mm in diameter, Parsivel² fall speed measurements matched closely with both terminal speed predictions and HOD fall speed measurements. For raindrops between about 1 and 3 mm in diameter, Parsivel² fall speed observations showed a notable deviation from terminal speed predictions. HOD fall speed measurements did not show this behavior. For raindrops larger than about 3 mm in diameter, Parsivel² observations approached closer to terminal speed predictions and HOD measurements with increasing raindrop diameter bins, exhibiting smaller deviations. To show that these observations for event 5 were similar to those for all of the rainfall events, averages of raindrop fall speed measurements for all of the observed rainfall events are presented in Fig. 7b. Parsivel² raindrop fall speed observations for all of the rainfall events are presented individually (later in Fig. 10) to further demonstrate that the deviation in Parsivel² fall speed measurements from terminal speed predictions follow a similar pattern for all of the events regardless of rain intensity and wind conditions.

To test the statistical significance of the deviations of both HOD and Parsivel² (pseudo level 2) mean fall speed measurements from terminal speed predictions by Eq. (1) that is based on GK49 laboratory data (V_{t_1}) and by Beard (1976) (V_{t_2}) individually for each diameter bin, four separate one-sample *t* tests with *p* value (probability of obtaining the observed results, assuming that the null hypothesis is true) of 0.05 significance level were performed for event 5. The reason for using predictions by two different terminal speed parameterizations in these analyses was to test whether or not different terminal speed parameterizations alter the statistical results. The *t* tests were performed under the assumption of a normal distribution in observed data. Later in Fig. 8, distributions of HOD and Parsivel² raindrop fall speed measurements for each diameter

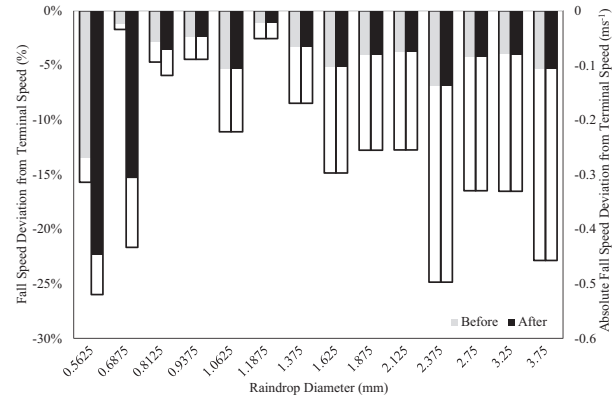


FIG. 6. Demonstration of the relative deviations (primary vertical axis) of HOD fall speed measurements from terminal speed predictions by Eq. (1) before (gray bars) and after (dark bars) implementation of Parsivel² filtering matrix to the HOD measurements for event 5. Absolute deviations (secondary vertical axis) of HOD fall speed measurements from terminal speed predictions before (hollow boxes attached to the gray bars) and after (hollow boxes attached to the dark bars) implementation of Parsivel² filtering matrix are also presented.

bin are shown. More than 68% of fall speed observations lie within one standard deviation of observed mean fall speeds for each diameter bin for both Parsivel² and HOD measurements, supporting the suitability of our normal distribution assumption. It should be noted that numbers of observed raindrops by HOD and Parsivel² are different for each diameter bin. The smaller number of raindrop observations by HOD as compared to those by Parsivel² was due to the HOD's smaller measurement volume (70 mm × 70 mm × 5.25 mm) that was customized for high measurement accuracy and its operating principles (i.e., sequential high-speed image storage and download) as described in Testik and Rahman (2016). The null hypotheses (H_0) for the tests for HOD and Parsivel² measurements were $H_0: \mu_{v_f}^{\text{HOD}} = V_{t_1}$, $H_0: \mu_{v_f}^{\text{HOD}} = V_{t_2}$, $H_0: \mu_{v_f}^{\text{Parsivel}} = V_{t_1}$, and $H_0: \mu_{v_f}^{\text{Parsivel}} = V_{t_2}$, respectively, where, $\mu_{v_f}^{\text{HOD}}$ and $\mu_{v_f}^{\text{Parsivel}}$ represent mean fall speed measurements by HOD and Parsivel², respectively, and V_{t_1} and V_{t_2} represent terminal fall speed predictions by Eq. (1) and Beard (1976), respectively. The test results are tabulated in Table 2. As can be seen from this table, the deviations of the Parsivel² mean fall speed measurements from both Eq. (1) and Beard (1976) terminal speed predictions were statistically significant for all diameter bins (*p* value < 0.05). The deviations for the HOD measurements from the terminal speed predictions were also statistically significant except for the diameter bins of 0.688, 0.813, 0.938, 1.188, and 3.75 mm. This statistical analysis also demonstrated that raindrop terminal speed predictions using two different sources, GK49 and Beard (1976), do not have any statistically significant (*p* value) effect on the results. Therefore, we used only terminal speed predictions by Eq. (1) that is based on GK49 in the rest of this article. To test the statistical significance of the differences between mean fall speed measurements by HOD and Parsivel²

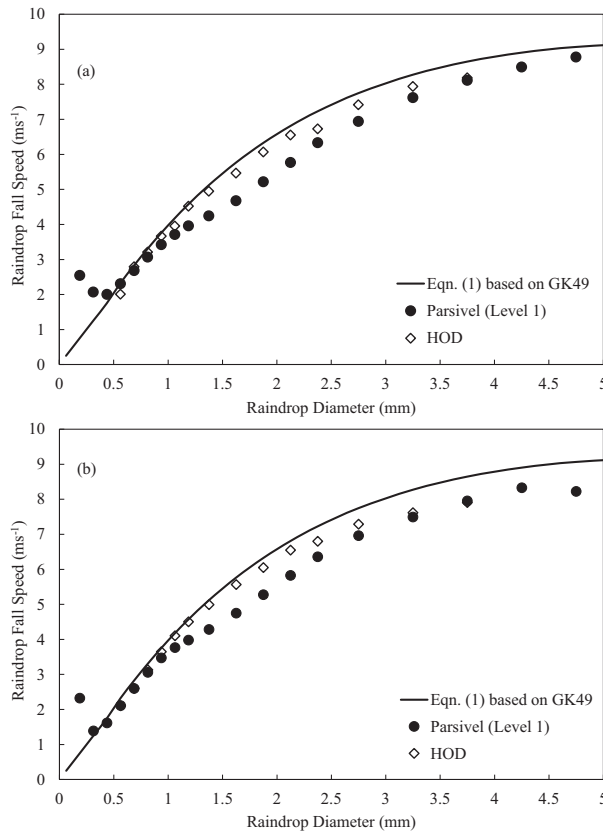


FIG. 7. Comparison of HOD-measured and Parsivel²-detected (level 1) raindrop fall speeds along with predicted terminal speeds by Eq. (1) based on GK49 for (a) event 5 and (b) all of the observed events. Fall speed values in (b) are averages of observations for all of the rainfall events.

($H_0: \mu_{v_f}^{\text{HOD}} = \mu_{v_f}^{\text{Parsivel}}$), a two-sample t test with 0.05 significance level was performed. The two-sample t -test results showed that the differences between raindrop fall speed measurements by these two disdrometers were statistically significant for all diameter bins > 0.5 mm, except for the diameter bins of 3.25 and 3.75 mm (Table 2). This finding provides sufficient evidence to state that Parsivel² raindrop fall speed measurements are significantly different from the HOD measurements.

Figure 8 shows a comparison of the raindrop fall speed distributions of event 5 for Parsivel² (pseudo level 2) and HOD measurements for each of the diameter bins. This figure demonstrates that, for each of the diameter bins, mean and median values of the Parsivel² measurements almost matched (near-symmetric distribution) whereas HOD measurements showed a skewed fall speed distribution toward subterminal values for the lower diameter bins of 0.563 and 0.689 mm. Moreover, this figure clearly demonstrates that deviations of the measured mean fall speeds from the terminal speed predictions were larger for Parsivel² measurements than for the HOD measurements. These deviations were so pronounced for Parsivel² measurements that the terminal speed predictions were beyond the standard deviation ranges for fall speed measurements for diameter bins of 1.188, 1.375, 1.625, 1.875,

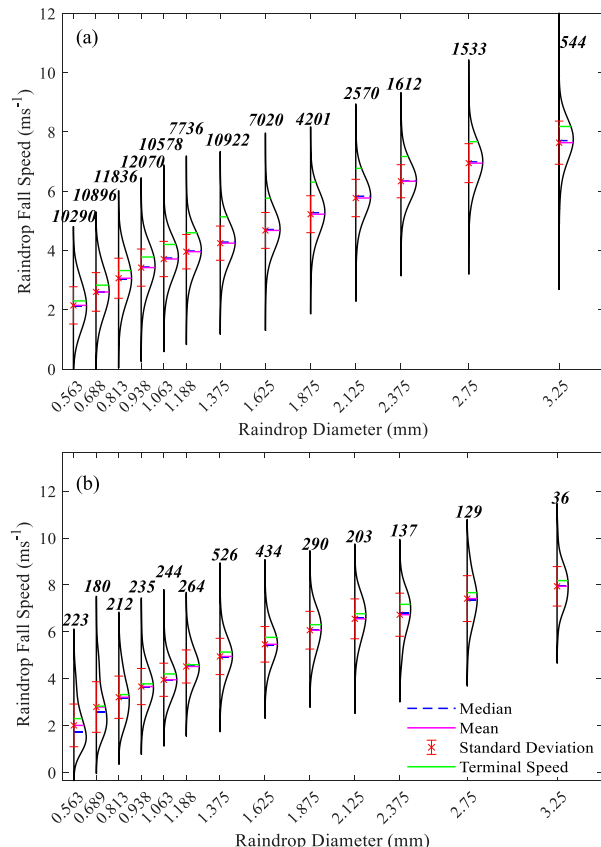


FIG. 8. Raindrop fall speed distributions for each diameter bin for (a) Parsivel² and (b) HOD measurements for event 5. Mean, median, and standard deviation of fall speed measurements and terminal speed predictions by Eq. (1) are also shown (see the legend). Numbers provided above the distributions for each diameter bin represent the number of raindrops in the corresponding diameter bin.

2.125, 2.375, and 2.75 mm. This was not the case for HOD measurements for any of the diameter bins (see Fig. 8). Figure 9 presents percentages of fall speed measurement deviations from the terminal speed predictions by Eq. (1) for each of the diameter bins for Parsivel² detected (level 1) and validated raindrops (pseudo level 2), and HOD observed raindrops for event 5. Since Parsivel² does not consider the smallest two diameter bins, we considered level 1 and pseudo level 2 data for 0.3125 mm and larger diameter bins. When compared to level 1 data, Parsivel² filtering matrix for this specific event reduced the fall speed deviation of pseudo level 2 data from terminal speed for the 0.3125 and 0.4375 mm diameter bins. On the other hand, Parsivel² filtering matrix caused increased deviations of Parsivel² pseudo level 2 data (as compared to level 1 data) between 0.5625 and 0.8125 mm diameter bins toward subterminal fall speeds (see Fig. 9). These results from Figs. 8 and 9 show that selective elimination of the Parsivel² filtering matrix yields an instrumental bias for fall speed measurements for the diameter bins between 0.3125 and 0.8125 mm. These biases may result in the underestimation of the number concentrations of small raindrop sizes.

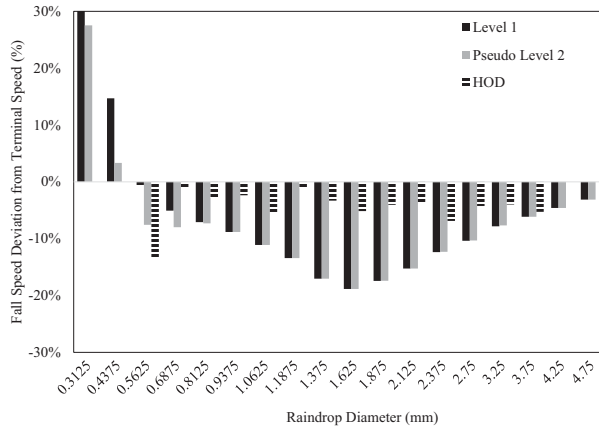


FIG. 9. Deviations of raindrop fall speed measurements from terminal speed predictions by Eq. (1) for Parsivel²-detected (level 1), Parsivel²-validated (pseudo level 2), and HOD observations for event 5. Here, the fall speed deviation for the 0.3125 mm diameter bin of level 1 data is 66%, exceeding the vertical axis value range shown in the figure.

It is evident from Fig. 9 that a bell-shaped deviation of Parsivel² measurements (both level 1 and 2 data) from terminal speed predictions by Eq. (1) for diameter bins between around 0.8125 and 3.25 mm with the maximum deviation at around 1.625 mm diameter bin. HOD measurements did not show such a bell-shaped deviation, but they were rather random within a range of 0% to -5%. We analyzed additional 5 rainfall events (see Table 1), taking into account various wind speed, rain intensity, and other environmental characteristics, in order to verify the findings presented in Fig. 9. Figure 10 presents measured raindrop fall speed deviations from terminal speed predictions by Eq. (1) for (Fig. 10a) Parsivel² detected (level 1), (Fig. 10b) Parsivel² validated (pseudo level 2), and (Fig. 10c) HOD measured raindrops for all observed rainfall events. As can be seen in this figure, although high wind speed and heavy rain intensity conditions enhanced raindrop fall speed deviations from predicted terminal speeds (for both Parsivel² and HOD observations), results for Parsivel² measured raindrop fall speed deviations for all of the observed rainfall events demonstrated a similar deviation trend consistently. Parsivel² filtering matrix disregarded raindrops having superterminal speeds, which occasionally worsened the average fall speed deviations from terminal speed predictions for the validated raindrops. For example, event 3 of Figs. 10a and 10b exhibited -4% and -10% measured fall speed deviations for the detected and validated raindrops, respectively, from predicted terminal speeds for the 0.3125 mm diameter bin. The impact of Parsivel² filtering matrix was evident on validated raindrop fall speed deviations up until 0.8125 mm diameter bin for all of the observed rainfall events and reduced the average fall speeds (see Figs. 10a,b). Differences in fall speed deviations of the detected and validated raindrops were not observed for diameter bins larger than 0.8125 mm diameter bin. Despite the differences in the rainfall event characteristics, deviations of measured raindrop fall speeds from terminal speed predictions for diameter bins

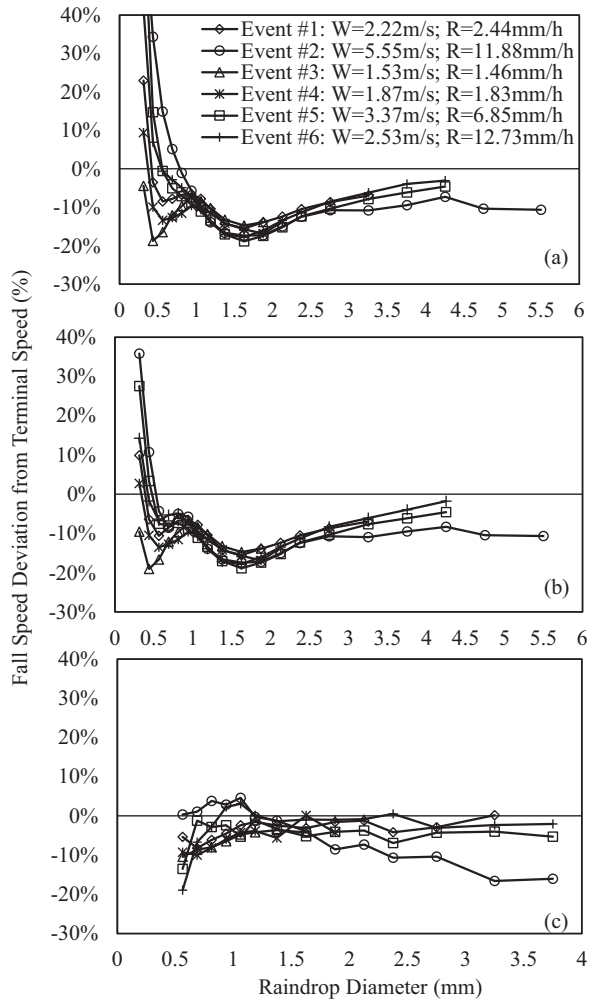


FIG. 10. Deviations of raindrop fall speed measurements from terminal speed predictions by Eq. (1) for (a) Parsivel²-detected (level 1), (b) Parsivel²-validated (pseudo level 2), and (c) HOD observations for all of the rainfall events in Table 1. Here, fall speed deviations for the 0.3125 mm diameter bin of level 1 data are 66%, 66%, and 42% for events 2, 5, and 6, respectively, exceeding the vertical axis value range shown in the figure. Average values for rain intensity (R) and wind speed (W) during the observed rainfall events are provided in the legend.

in between around 0.8125 and 3.25 mm showed similar bell-shaped deviations for both Parsivel² detected and Parsivel² validated raindrops (see Figs. 10a,b). Such a deviation pattern was not present for HOD fall speed measurements (Fig. 10c). Given that results presented in the rest of the article are also consistent for all of the observed rainfall events similar to the consistency in the results presented in Fig. 10, the rest of the results are presented only for event 5 for space and clarity considerations.

There may be several potential causes for this observed bell-shaped deviation behavior for Parsivel² measurements, including limitations of the laser sensor, rainfall microphysical processes (e.g., raindrop oscillations), Parsivel² filtering

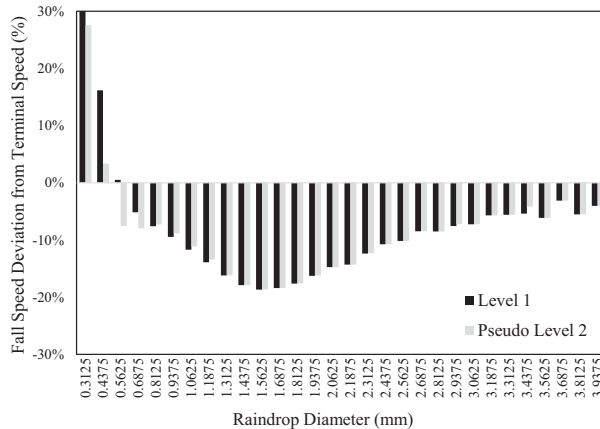


FIG. 11. Deviations of Parsivel²-detected (level 1) and -validated (pseudo level 2) fall speed measurements from predicted terminal speed by Eq. (1) for event 5. Deviations are presented for a fixed diameter bin width of 0.125 mm. Here, the fall speed deviation for the 0.3125 mm diameter bin of level 1 data is 66%, exceeding the vertical axis value range shown in the figure.

matrix, and nonuniform bin sizes. Figure 9 shows that level 1 and pseudo level 2 data have nearly identical deviations from the terminal speed predictions, demonstrating that Parsivel² filtering matrix is not responsible for this observation. To evaluate the possibility of nonuniform bin sizing as a potential cause of this observation, we reanalyzed rainfall observations of event 5 with uniform bin widths of 0.125 mm and presented in Fig. 11. As can be seen in this figure, uniform bin selection resulted in similar bell-shaped deviation, demonstrating that nonuniform bin sizing is not responsible for this observation. Furthermore, since HOD measurements, for which we can also visually observe individual raindrop behavior, did not show bell-shaped deviations for the same rainfall events, we can also eliminate rainfall microphysics as a potential cause of the bell-shaped deviations seen in Fig. 9 for the Parsivel² fall speed measurements. Note that our laboratory experimental observations by Parsivel² also showed the same bell-shaped deviation pattern from terminal speed predictions, which implies that we can disregard the outdoor environmental factors such as wind, temperature, humidity for the observed pattern. Therefore, we conclude that the laser characteristics and fall speed calculation methodology from laser sensor data are the potential causes for the bell-shaped deviation pattern. As examples of the laser characteristics, nonuniformity of the laser sheet thickness and laser sampling frequency that determines the raindrop fall time in the laser sheet are potential causes for fall speed measurement inaccuracies due to the fall speed calculation methodology for such sensors. Since we did not have the ability to test the Parsivel² laser sheet thickness for uniformity, we cannot make a relevant conclusion. Assuming a uniform laser sheet thickness of 1 mm as noted by Parsivel² documentation (OTT 2017) and using Eq. (1) terminal speed predictions for different raindrop sizes ($D = 0.5\text{--}5\text{ mm}$), one can calculate that a raindrop would be observed from 5 to 21 times by the sensor. Therefore, one can expect fall speed measurement errors around 5%–18%,

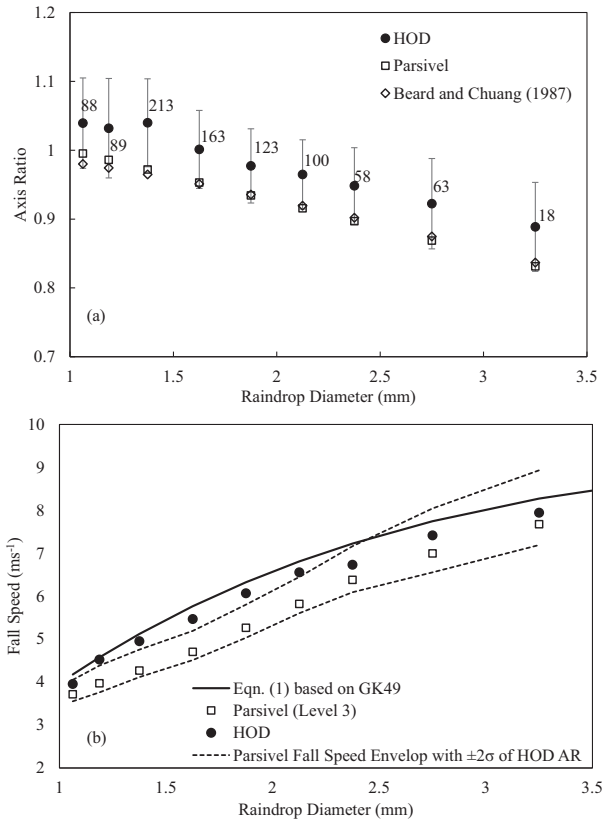


FIG. 12. (a) HOD raindrop axis ratio measurements (solid circles) presented with ± 1 standard deviation (vertical bars) and number of raindrops (next to vertical bars) for each of the diameter bins larger than 1 mm along with Parsivel²-assumed axis ratio values (open squares) and predicted axis ratio values by Beard and Chuang's (1987) model (open diamonds). (b) Parsivel² fall speed measurements are presented with an envelope of ± 2 standard deviations of HOD axis ratio measurements for each of the diameter bins.

depending on the raindrop size, solely due to laser sampling frequency (50 kHz). As an example of the fall speed calculation methodology, there are inherent assumptions (in particular raindrop shape assumptions) for fall speed calculations using laser measurements with significant potential for measurement inaccuracies. For diameters less than 1 mm, Parsivel² assumes that raindrops are spherical, whereas for diameters between 1 and 5 mm, raindrops are assumed to be oblate spheroids with axis ratios decreasing linearly from 1 to 0.7 with increasing diameter and reaching an axis ratio of 0.7 for raindrops larger than 5 mm (Battaglia et al. 2010). This axis ratio distribution may not accurately represent the axis ratios of actual observations. Figure 12a shows HOD axis ratio measurements with ± 1 standard deviations (shown as vertical bars) for raindrops larger than 1 mm along with the assumed axis ratios in Parsivel² calculations and predicted axis ratios by the analytical model of Beard and Chuang (1987). It is evident from Fig. 12a that while Parsivel² assumed axis ratios are close to the predictions by Beard and Chuang (1987), they distinctly differ from mean values of the actual raindrop axis ratio measurements by the HOD

and lie within the close proximity of the lower bounds of standard deviations for HOD measured raindrop axis ratios. To show the impacts of assumed axis ratio values in Parsivel² fall speed measurements, Fig. 12b presents Parsivel² fall speed measurements (level 3 data) with an envelope that is calculated by Parsivel² level 1 data and using HOD measured axis ratios with ± 2 standard deviations. While Fig. 12 demonstrates the significant impact of assumed raindrop axis ratio distribution in Parsivel² fall speed, it also demonstrates that assumed axis ratio distribution may not be fully responsible for the observed deviations from the GK49 terminal speed predictions [Eq. (1)] and there are likely other factors contributing such as laser sampling frequency as discussed. Furthermore, we conducted a two-sample *t* test with the hypothesis as equal mean fall speeds for HOD measurements and Parsivel² measurements with raindrop axis ratio distribution assumed to be ± 2 standard deviations of HOD measured axis ratio distribution. The results of this test revealed that differences in mean fall speeds by the two instruments were statistically significant for raindrops within the 1 mm–2.125 m diameter range, where bell-shaped deviation pattern was observed.

Parsivel² DSD measurements have been a pillar for a large number of studies for different applications. Given that Parsivel² DSD calculations rely on the fall speed measurements with the aforementioned limitations, the relevant impacts on the accuracy of Parsivel² DSD measurements grant a discussion. DSD computations for this discussion were conducted using the following formulation in Eq. (2), where $N(D)_i$ (m⁻³ mm⁻¹) is the raindrop number concentration per unit volume for the *i*th raindrop diameter bin (Raupach and Berne 2015):

$$N(D)_i = \frac{1}{A_i \Delta D_i \Delta t} \sum_{j=1}^{j=32} \frac{C_{j,i}}{v_j}. \quad (2)$$

Here, $C_{j,i}$ is the number of raindrop observations in the *i*th diameter bin and *j*th fall velocity bin during the time interval $\Delta t(s)$, ΔD_i is the width of the *i*th diameter bin (mm), v_j is the mean fall velocity of the *j*th velocity bin (m s⁻¹), and A_i is the effective measurement area (m²) of Parsivel² for the *i*th diameter bin. While the actual measurement area of Parsivel² is 180 mm \times 30 mm, raindrops passing through the rectangular measurement area partially (i.e., at the edges of the area) are omitted. Therefore, the effective measurement area, A_i (in m²), depends on the raindrop diameter bin as follows:

$$A_i = 10^{-6} \times 180 \times \left(30 - \frac{D_i}{2}\right). \quad (3)$$

Here, D_i is the midbin diameter (in mm) for the *i*th diameter bin. Underestimation bias observed for Parsivel² raindrop fall speed measurements for diameters larger than 0.8125 mm (see Fig. 9) would introduce an overestimation bias for Parsivel² DSD measurements [$N(D)$ in mm⁻¹ m⁻³] due to their inverse mathematical relationship in calculating the $N(D)$ values. Here, we present event 5 to demonstrate the impact of Parsivel² fall speed measurements on the Parsivel² reported DSDs; however, it should be noted that all of the observed rainfall events show the same impact. To demonstrate the effect of fall speed

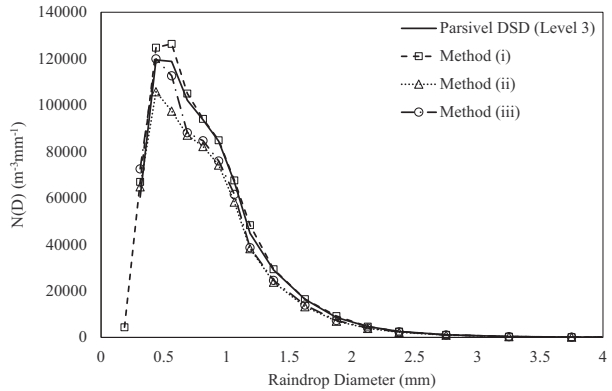


FIG. 13. Comparison among Parsivel² given DSD (level 3) with the DSDs estimated based on Parsivel²-detected (level 1) raindrop diameter and fall speed measurements [method (i)], Parsivel²-validated raindrop counts (level 2) with terminal speed predictions by Eq. (1) [method (ii)], and HOD-measured fall speeds [method (iii)] for event 5.

measurements on DSD calculations, Fig. 13 presents DSDs calculated in the following 3 different ways and compare them with the Parsivel² reported DSD measurements (level 3): (i) using Parsivel² detected raindrop diameter and fall speed measurements (level 1), (ii) using Parsivel² validated raindrop counts (level 2) with terminal speed predictions by Eq. (1) for middiameter values of each diameter bin, and (iii) using Parsivel² validated raindrop counts (level 2) with average fall speed measurements by the HOD for each of the diameter bins. As can be seen from this comparison, Parsivel² reported $N(D)$ values are larger than those calculated by (ii) and (iii) for diameter bins larger than 0.5625 mm. For the diameter bin range between 0.3125 and 0.8125 mm, Parsivel² reported $N(D)$ values are smaller than those calculated by (i) for the level 1 detected raindrops. Recall that this diameter range for level 1 data corresponds to the diameter bins with fast-falling raindrop observations that were eliminated by the Parsivel² filtering matrix, demonstrating the impact of Parsivel² filtering matrix in the reported DSD measurements. Figure 14 presents the relative bias of a typical Parsivel² reported DSD with the DSDs calculated using methods (ii) and (iii). Similar to the bell-shaped fall speed deviation pattern (see Fig. 9), Fig. 14 clearly demonstrates the presence of a bell-shaped distribution in around the 0.812–3.75 mm diameter bins with the maximum relative bias of 25% at the diameter bin of 1.625 mm.

Kinetic energy of raindrops falling on ground has been widely recognized as a potential indicator of soil erosion, and Parsivel² measurements have often been utilized in soil erosion studies for kinetic energy estimations (e.g., Angulo-Martínez and Barros 2015). Therefore, we also investigated the impacts of Parsivel² fall speed measurements on rainfall kinetic energy calculations. Time-specific kinetic energy of rainfall (KE with units of J m⁻² h⁻¹) is calculated as (Salles et al. 2002)

$$KE_{D_i} = \left(\frac{\pi}{12}\right) \left(\frac{1}{10^6}\right) \left(\frac{3600}{t}\right) \left(\frac{1}{A_i}\right) n_i D_i^3 (v_{D_i})^2. \quad (4)$$

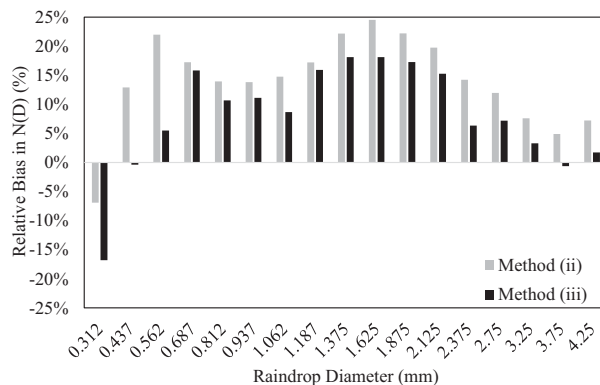


FIG. 14. Estimated relative bias of Parsivel² given DSD (level 3) with respect to calculated DSDs based on Parsivel²-validated raindrop counts (level 2) with terminal speed predictions by Eq. (1) [method (ii)] and HOD-measured fall speeds [method (iii)] for event 5.

Here, n_i is the number of raindrops counted in the i th diameter bin during the time interval t (s), D_i (mm) and v_{D_i} are the midvalue of the i th diameter bin and average raindrop fall speed (m s^{-1}) for the i th diameter bin, respectively, and KE_{D_i} is the time-specific kinetic energy for the i th diameter bin. Figure 15 presents KE_{D_i} values for event 5 that were calculated using methods (i)–(iii) described earlier and also using pseudo level 2 data. Figure 15 shows that there are major discrepancies in the calculated KE_{D_i} values using different methods with different measured and predicted fall speed values as KE is directly proportional to the square of raindrop fall speed. The discrepancies between the calculated KE_{D_i} values using pseudo level 2 data and those using methods (ii) and (iii) are particularly notable for the raindrop diameter bins between 0.812 and 3.75 mm. This is due to the bell-shaped deviations of Parsivel² fall speed measurements from terminal speed predictions in this diameter range (see Fig. 9), which is an instrumental artifact as discussed earlier. There were no noticeable differences between calculated KE_{D_i} values by

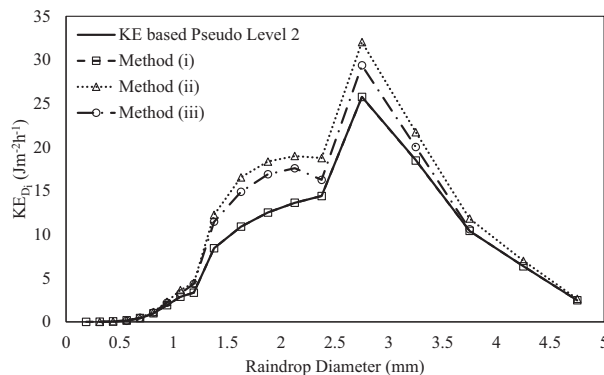


FIG. 15. Comparison among calculated KE_{D_i} values using different methods for event 5. KE_{D_i} values were calculated using pseudo level 2 data, level 1 data [method (i)], level 2 data with terminal speed predictions by Eq. (1) [method (ii)], and level 2 data with HOD fall speed measurements [method (iii)] (see the legend).

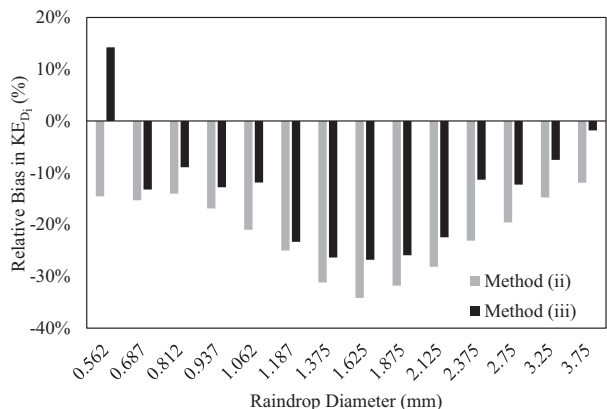


FIG. 16. Estimated relative bias of KE_{D_i} calculations using pseudo level 2 data with respect to KE_{D_i} calculations using method (ii) [level 2 data with terminal speed predictions by Eq. (1)] and method (iii) (level 2 data with HOD measured fall speeds) for event 5.

level 1 and pseudo level 2 data. This was because the fall speed differences between these two data levels were mainly for raindrop diameter bins smaller than 1 mm that are created by the application of the Parsivel² filtering matrix (see Fig. 5), which leads to only small differences in calculated KE values.

Relative biases in KE_{D_i} calculations using Parsivel² pseudo level 2 data with respect to those calculations using methods (ii) and (iii) are presented in Fig. 16. This figure clearly demonstrates the effects of Parsivel² fall speed measurements on calculated KE_{D_i} values and indicates that the effects are observed for the same raindrop diameter bin range of approximately 0.812 to 3.75 mm, within which the bell-shaped fall speed deviations are present (see Fig. 9). The maximum bias occurs at the diameter bin of 1.625 mm, which is the same diameter bin for the maximum fall speed deviations (see Fig. 9). The maximum relative bias of calculated KE_{D_i} values for event 5 shown in this figure were -34% and -27% with respect to methods (ii) and (iii), respectively. Therefore, it is expected that Parsivel² fall speed measurements result in notable underestimation of the KE values with potential impacts on rain-induced soil erosion estimations and other applications.

4. Conclusions

Capabilities of Parsivel² disdrometer for raindrop fall speed measurements with potential impacts on DSD measurements were assessed. For this purpose, rainfall microphysical observations were conducted using collocated Parsivel² and HOD disdrometers, both optical-type disdrometers with different working principles, during 6 rainfall events. These rainfall events covered a wide range of rainfall rate, wind speed, temperature, and humidity; and hence, our evaluations utilized disdrometer data collected under a variety of meteorological conditions.

In assessing the measurement capabilities of Parsivel², our efforts involved faithful identification of the data processing

algorithm, which is not available by the manufacturer and in the literature. We would like to note that there were no discussions with the manufacturer on this study and no funding support from the manufacturer for this study. We have identified that Parsivel² implements a filtering process of the detected particles and validates them as raindrops using criteria that can be presented in a matrix form (i.e., Parsivel² filtering matrix in Fig. 3). Through laboratory experiments, which were later verified using field observations, we faithfully identified the Parsivel² filtering matrix that is used to process the level 1 data to form the level 2 data. An important consequence of the Parsivel² filtering matrix is that it eliminates faster-falling detected particles within the diameter bins smaller than 0.8125 mm, hence, creating a bias in fall speed measurements for those small diameter bins by bringing the mean fall speed values down without an observational evidence. We also faithfully identified the fall speed calculation methodology by Parsivel² and revealed that midvalues of the fall speed bin are used, instead of measured fall speeds of individual raindrops, in relevant calculations. A potential consequence of this, although not investigated in this study, is the quantization errors in DSD and other rain parameter calculations due to the nonuniform Parsivel² fall speed bin widths that increase up to 3.2 m s^{-1} for the higher end of the fall speed bins. Future research on this can document potential errors and means to avoid such errors, if present, by calculation methodologies using individual raindrops fall speed measurements.

Our investigation revealed that Parsivel² fall speed measurements exhibit a bell-shaped deviation from terminal speed predictions by Eq. (1) for raindrop sizes between around 0.8125 and 3.25 mm diameter bins. The peak of the bell shape was at around 1.625 mm diameter bin. This deviation pattern was consistent for the Parsivel² measurements from all of the rainfall events and laboratory experiments, indicating that this was independent of the meteorological conditions. Furthermore, such a deviation pattern was absent for the HOD measurements from all of the events, which led us to the conclusion that the observed deviation pattern is an instrumental artifact. As discussed in section 3 with considerations of different potential causes, our conclusion is that Parsivel² laser sensor/sheet characteristics was responsible for the bell-shaped deviations. The systematic deviations of fall speed measurements as compared to the GK49 terminal speed predictions and HOD measurements have downstream impacts in processed Parsivel² data, in particular in Parsivel² DSD observations and KE calculations. Comparisons of Parsivel² reported DSDs with the DSDs calculated using Parsivel² raindrop counts and terminal speed predictions using Eq. (1) as well as HOD measured fall speeds revealed the presence of relative bias of Parsivel² reported DSDs similar to the bell-shaped fall speed deviation pattern for the same diameter range. KE values calculated using Parsivel² fall speed measurements showed a similar behavior. Since KE is directly proportional to the square of raindrop fall speed, we observed a substantial underestimation of the calculated KE values using Parsivel² fall speed measurements as compared to those calculated using

both terminal speed predictions by Eq. (1) and HOD fall speed measurements. The relative biases for KE values calculated using Parsivel² fall speed measurements were a clear reflection of the bell-shaped fall speed deviations in Parsivel² measurements.

Level 1 data and Parsivel² filtering matrix are not available to the Parsivel² users through the commercially available software and only level 2 and level 3 data are available. Processing of data from level 1 to level 2 and from level 2 to level 3 conceals potential instrumental artifacts and data processing information is critical to the Parsivel² users and data beneficiaries. Parsivel² internal calculation algorithm, including the filtering matrix, faithfully identified in this study reveals the data processing methodology, which can be considered as a “black box” for the user community. Identified data processing methodology is of great importance to the Parsivel² data users and beneficiaries in interpretations of the observations, understanding the instrumental limitations, and development of methodologies for data improvements, among various other implementations.

Acknowledgments. This research was supported by the funds provided by the National Science Foundation under Grant AGS-1741250 to the second author (FYT). The first author is a graduate student under the guidance of FYT. This study was conducted independent of the manufacturer of the OTT Parsivel² disdrometer, and there were no funds provided by the manufacturer.

Data availability statement. Data presented in this article will be made available upon reasonable request from the corresponding author (Dr. Firat Y. Testik) and after completion of a fair use agreement.

REFERENCES

Angulo-Martínez, M., and A. P. Barros, 2015: Measurement uncertainty in rainfall kinetic energy and intensity relationships for soil erosion studies: An evaluation using Parsivel disdrometers in the southern Appalachian Mountains. *Geomorphology*, **228**, 28–40, <https://doi.org/10.1016/j.geomorph.2014.07.036>.

—, S. Beguería, B. Latorre, and M. Fernández-Raga, 2018: Comparison of precipitation measurements by OTT Parsivel² and Thies LPM optical disdrometers. *Hydrol. Earth Syst. Sci.*, **22**, 2811–2837, <https://doi.org/10.5194/hess-22-2811-2018>.

Aoki, M., H. Iwai, K. Nakagawa, S. Ishii, and K. Mizutani, 2016: Measurements of rainfall velocity and raindrop size distribution using coherent Doppler lidar. *J. Atmos. Oceanic Technol.*, **33**, 1949–1966, <https://doi.org/10.1175/JTECH-D-15-0111.1>.

Awaka, J., M. Le, V. Chandrasekar, N. Yoshida, T. Higashiuwatoko, T. Kubota, and T. Iguchi, 2016: Rain type classification algorithm module for GPM Dual-Frequency Precipitation Radar. *J. Atmos. Oceanic Technol.*, **33**, 1887–1898, <https://doi.org/10.1175/JTECH-D-16-0016.1>.

Baire, Q., and Coauthors, 2022: Calibration uncertainty of non-catching precipitation gauges. *Sensors*, **22**, 6413, <https://doi.org/10.3390/s22176413>.

Battaglia, A., E. Rustemeier, A. Tokay, U. Blahak, and C. Simmer, 2010: Parsivel snow observations: A critical assessment.

J. Atmos. Oceanic Technol., **27**, 333–344, <https://doi.org/10.1175/2009JTECHA1332.1>.

Beard, K. V., 1976: Terminal velocity and shape of cloud and precipitation drops aloft. *J. Atmos. Sci.*, **33**, 851–864, [https://doi.org/10.1175/1520-0469\(1976\)033<0851:TVASOC>2.0.CO;2](https://doi.org/10.1175/1520-0469(1976)033<0851:TVASOC>2.0.CO;2).

—, 1977: Terminal velocity adjustment for cloud and precipitation drops aloft. *J. Atmos. Sci.*, **34**, 1293–1298, [https://doi.org/10.1175/1520-0469\(1977\)034<1293:TVAFCA>2.0.CO;2](https://doi.org/10.1175/1520-0469(1977)034<1293:TVAFCA>2.0.CO;2).

—, and C. Chuang, 1987: A new model for the equilibrium shape of raindrops. *J. Atmos. Sci.*, **44**, 1509–1524, [https://doi.org/10.1175/1520-0469\(1987\)044<1509:ANMFTE>2.0.CO;2](https://doi.org/10.1175/1520-0469(1987)044<1509:ANMFTE>2.0.CO;2).

Blanchard, D. C., 1950: The behavior of water drops at terminal velocity in air. *Eos, Trans. Amer. Geophys. Union*, **31**, 836–842, <https://doi.org/10.1029/TR031i006p00836>.

Brandes, E. A., G. Zhang, and J. Vivekanandan, 2002: Experiments in rainfall estimation with a polarimetric radar in a subtropical environment. *J. Appl. Meteor.*, **41**, 674–685, [https://doi.org/10.1175/1520-0450\(2002\)041<0674:EIREWA>2.0.CO;2](https://doi.org/10.1175/1520-0450(2002)041<0674:EIREWA>2.0.CO;2).

Cotton, W. R., and R. A. Anthes, 1992: *Storm and Cloud Dynamics*. Vol. 44, Academic Press, 883 pp.

Epema, G. F., and H. T. Riezebos, 1983: Fall velocity of water-drops at different heights as a factor influencing erosivity of simulated rain. *Rainfall Simulation Runoff and Soil Erosion*, Catena Verlag, 1–17.

Friedrich, K., S. Higgins, F. J. Masters, and C. R. Lopez, 2013: Articulating and stationary Parsivel disdrometer measurements in conditions with strong winds and heavy rainfall. *J. Atmos. Oceanic Technol.*, **30**, 2063–2080, <https://doi.org/10.1175/JTECH-D-12-00254.1>.

Gunn, R., and G. D. Kinzer, 1949: The terminal velocity of fall for water droplets in stagnant air. *J. Meteor.*, **6**, 243–248, [https://doi.org/10.1175/1520-0469\(1949\)006<0243:TTVOFF>2.0.CO;2](https://doi.org/10.1175/1520-0469(1949)006<0243:TTVOFF>2.0.CO;2).

Habib, E., W. F. Krajewski, and G. J. Ciach, 2001: Estimation of rainfall interstation correlation. *J. Hydrometeor.*, **2**, 621–629, [https://doi.org/10.1175/1525-7541\(2001\)002<0621:EORIC>2.0.CO;2](https://doi.org/10.1175/1525-7541(2001)002<0621:EORIC>2.0.CO;2).

Hosking, J. G., and C. D. Stow, 1991: Ground-based measurements of raindrop fall speeds. *J. Atmos. Oceanic Technol.*, **8**, 137–147, [https://doi.org/10.1175/1520-0426\(1991\)008<0137:GBMORF>2.0.CO;2](https://doi.org/10.1175/1520-0426(1991)008<0137:GBMORF>2.0.CO;2).

Jaffrain, J., and A. Berne, 2011: Experimental quantification of the sampling uncertainty associated with measurements from Parsivel disdrometers. *J. Hydrometeor.*, **12**, 352–370, <https://doi.org/10.1175/2010JHM1244.1>.

Jayawardena, A. W., and R. B. Rezaur, 2000: Measuring drop size distribution and kinetic energy of rainfall using a force transducer. *Hydrol. Processes*, **14**, 37–49, [https://doi.org/10.1002/\(SICI\)1099-1085\(200001\)14:1<37::AID-HYP908>3.0.CO;2-M](https://doi.org/10.1002/(SICI)1099-1085(200001)14:1<37::AID-HYP908>3.0.CO;2-M).

Kruger, A., and W. F. Krajewski, 2002: Two-dimensional video disdrometer: A description. *J. Atmos. Oceanic Technol.*, **19**, 602–617, [https://doi.org/10.1175/1520-0426\(2002\)019<0602:TDVDAD>2.0.CO;2](https://doi.org/10.1175/1520-0426(2002)019<0602:TDVDAD>2.0.CO;2).

Lanza, L. G., and E. Vuerich, 2009: The WMO field intercomparison of rain intensity gauges. *Atmos. Res.*, **94**, 534–543, <https://doi.org/10.1016/j.atmosres.2009.06.012>.

—, and Coauthors, 2021: Calibration of non-catching precipitation measurement instruments: A review. *Meteor. Appl.*, **28**, e2002, <https://doi.org/10.1002/met.2002>.

Laws, J. O., 1941: Measurements of the fall-velocity of water-drops and raindrops. *Eos, Trans. Amer. Geophys. Union*, **22**, 709–721, <https://doi.org/10.1029/TR022i003p00709>.

Lin, L., X. Bao, S. Zhang, B. Zhao, and W. Xia, 2021: Correction to raindrop size distributions measured by Parsivel disdrometers in strong winds. *Atmos. Res.*, **260**, 105728, <https://doi.org/10.1016/j.atmosres.2021.105728>.

Loh, J. L., D.-I. Lee, and C.-H. You, 2019: Inter-comparison of DSDs between Jincheon and Miryang at South Korea. *Atmos. Res.*, **227**, 52–65, <https://doi.org/10.1016/j.atmosres.2019.04.031>.

Montero-Martínez, G., and F. García-García, 2016: On the behaviour of raindrop fall speed due to wind. *Quart. J. Roy. Meteor. Soc.*, **142**, 2013–2020, <https://doi.org/10.1002/qj.2794>.

—, A. B. Kostinski, R. A. Shaw, and F. García-García, 2009: Do all raindrops fall at terminal speed? *Geophys. Res. Lett.*, **36**, L11818, <https://doi.org/10.1029/2008GL037111>.

Nešpor, V., W. F. Krajewski, and A. Kruger, 2000: Wind-induced error of raindrop size distribution measurement using a two-dimensional video disdrometer. *J. Atmos. Oceanic Technol.*, **17**, 1483–1492, [https://doi.org/10.1175/1520-0426\(2000\)017<1483:WIEORS>2.0.CO;2](https://doi.org/10.1175/1520-0426(2000)017<1483:WIEORS>2.0.CO;2).

OTT, 2017: Present Weather Sensor OTT Parsivel². OTT, 52 pp., <https://www.ott.com/download/operating-instructions-present-weather-sensor-ott-parsivel2-with-screen-heating-1>.

Park, S.-G., H.-L. Kim, Y.-W. Ham, and S.-H. Jung, 2017: Comparative evaluation of the OTT Parsivel² using a collocated two-dimensional video disdrometer. *J. Atmos. Oceanic Technol.*, **34**, 2059–2082, <https://doi.org/10.1175/JTECH-D-16-0256.1>.

Pei, B., F. Y. Testik, and M. Gebremichael, 2014: Impacts of raindrop fall velocity and axis ratio errors on dual-polarization radar rainfall estimation. *J. Hydrometeor.*, **15**, 1849–1861, <https://doi.org/10.1175/JHM-D-13-0201.1>.

Pinsky, M. B., and A. P. Khain, 1996: Simulations of drop fall in a homogeneous isotropic turbulent flow. *Atmos. Res.*, **40**, 223–259, [https://doi.org/10.1016/0169-8095\(95\)00047-X](https://doi.org/10.1016/0169-8095(95)00047-X).

Pruppacher, H. R., and J. D. Klett, 2012: *Microphysics of Clouds and Precipitation*. Springer, 714 pp.

Raupach, T. H., and A. Berne, 2015: Correction of raindrop size distributions measured by Parsivel disdrometers, using a two-dimensional video disdrometer as a reference. *Atmos. Meas. Tech.*, **8**, 343–365, <https://doi.org/10.5194/amt-8-343-2015>.

Salles, C., J. Poesen, and D. Sempere-Torres, 2002: Kinetic energy of rain and its functional relationship with intensity. *J. Hydrol.*, **257**, 256–270, [https://doi.org/10.1016/S0022-1694\(01\)00555-8](https://doi.org/10.1016/S0022-1694(01)00555-8).

Testik, F. Y., and A. P. Barros, 2007: Toward elucidating the microstructure of warm rainfall: A survey. *Rev. Geophys.*, **45**, RG2003, <https://doi.org/10.1029/2005RG000182>.

—, and M. K. Rahman, 2016: High-speed optical disdrometer for rainfall microphysical observations. *J. Atmos. Oceanic Technol.*, **33**, 231–243, <https://doi.org/10.1175/JTECH-D-15-0098.1>.

—, and B. Pei, 2017: Wind effects on the shape of raindrop size distribution. *J. Hydrometeor.*, **18**, 1285–1303, <https://doi.org/10.1175/JHM-D-16-0211.1>.

—, A. P. Barros, and L. F. Bliven, 2006: Field observations of multimode raindrop oscillations by high-speed imaging. *J. Atmos. Sci.*, **63**, 2663–2668, <https://doi.org/10.1175/JAS3773.1>.

Thurai, M., W. A. Petersen, A. Tokay, C. Schultz, and P. Gatlin, 2011: Drop size distribution comparisons between Parsivel and 2-D video disdrometers. *Adv. Geosci.*, **30**, 3–9, <https://doi.org/10.5194/adgeo-30-3-2011>.

—, V. N. Bringi, W. A. Petersen, and P. N. Gatlin, 2013: Drop shapes and fall speeds in rain: Two contrasting examples. *J. Appl. Meteor. Climatol.*, **52**, 2567–2581, <https://doi.org/10.1175/JAMC-D-12-085.1>.

Tokay, A., A. Kruger, and W. F. Krajewski, 2001: Comparison of drop size distribution measurements by impact and optical

disdrometers. *J. Appl. Meteor.*, **40**, 2083–2097, [https://doi.org/10.1175/1520-0450\(2001\)040<2083:CODSDM>2.0.CO;2](https://doi.org/10.1175/1520-0450(2001)040<2083:CODSDM>2.0.CO;2).

—, W. A. Petersen, P. Gatlin, and M. Wingo, 2013: Comparison of raindrop size distribution measurements by collocated disdrometers. *J. Atmos. Oceanic Technol.*, **30**, 1672–1690, <https://doi.org/10.1175/JTECH-D-12-00163.1>.

—, D. B. Wolff, and W. A. Petersen, 2014: Evaluation of the new version of the laser-optical disdrometer, OTT Parsivel². *J. Atmos. Oceanic Technol.*, **31**, 1276–1288, <https://doi.org/10.1175/JTECH-D-13-00174.1>.

Upton, G., and D. Brawn, 2008: An investigation of factors affecting the accuracy of Thies disdrometers. *WMO Technical Conf. on Instruments and Methods of Observation*, Saint Petersburg, Russia, WMO, 27–29, [https://library.wmo.int/pmb_ged/wmo-td_1462_en/2\(10\)_Upton_United_Kingdom.pdf](https://library.wmo.int/pmb_ged/wmo-td_1462_en/2(10)_Upton_United_Kingdom.pdf).

Yu, C.-K., P.-R. Hsieh, S. E. Yuter, L.-W. Cheng, C.-L. Tsai, C.-Y. Lin, and Y. Chen, 2016: Measuring droplet fall speed with a high-speed camera: Indoor accuracy and potential outdoor applications. *Atmos. Meas. Tech.*, **9**, 1755–1766, <https://doi.org/10.5194/amt-9-1755-2016>.

Yuter, S. E., D. E. Kingsmill, L. B. Nance, and M. Löffler-Mang, 2006: Observations of precipitation size and fall speed characteristics within coexisting rain and wet snow. *J. Appl. Meteor. Climatol.*, **45**, 1450–1464, <https://doi.org/10.1175/JAM2406.1>.